Hearing Research 449 (2024) 109032

Contents lists available at ScienceDirect

Hearing Research

journal homepage: www.elsevier.com/locate/heares

Congenital deafness reduces alpha-gamma cross-frequency coupling in the auditory cortex

Prasandhya A. Yusuf [a,b,*], Peter Hubka [a], Wiebke Konerding [a], Rüdiger Land [a], Jochen Tillein [c], Andrej Kral [a,d]

[a] Hannover Medical School, Institute of AudioNeuroTechnology and Department of Experimental Otology of the ENT Clinics, Hannover, Germany
[b] Faculty of Medicine University of Indonesia, Department of Medical Physiology and Biophysics / Medical Technology IMERI, Jakarta, Indonesia
[c] J.W. Goethe University, Department of Otorhinolaryngology, Frankfurt am Main, Germany
[d] Australian Hearing Hub, School of Medicine and Health Sciences, Macquarie University, Sydney, Australia

ARTICLE INFO

Keywords:
Cochlear implant
Theta band
Alpha band
Hearing loss
Connectivity
Development

ABSTRACT

Neurons within a neuronal network can be grouped by bottom-up and top-down influences using synchrony in neuronal oscillations. This creates the representation of perceptual objects from sensory features. Oscillatory activity can be differentiated into stimulus-phase-locked (evoked) and non-phase-locked (induced). The former is mainly determined by sensory input, the latter by higher-level (cortical) processing. Effects of auditory deprivation on cortical oscillations have been studied in congenitally deaf cats (CDCs) using cochlear implant (CI) stimulation. CI-induced alpha, beta, and gamma activity were compromised in the auditory cortex of CDCs. Furthermore, top-down information flow between secondary and primary auditory areas in hearing cats, conveyed by induced alpha oscillations, was lost in CDCs. Here we used the matching pursuit algorithm to assess components of such oscillatory activity in local field potentials recorded in primary field A1. Additionally to the loss of induced alpha oscillations, we also found a loss of evoked theta activity in CDCs. The loss of theta and alpha activity in CDCs can be directly related to reduced high-frequency (gamma-band) activity due to cross-frequency coupling. Here we quantified such cross-frequency coupling in adult 1) hearing-experienced, acoustically stimulated cats (aHCs), 2) hearing-experienced cats following acute pharmacological deafening and subsequent CIs, thus in electrically stimulated cats (eHCs), and 3) electrically stimulated CDCs. We found significant cross-frequency coupling in all animal groups in $>$ 70% of auditory-responsive sites. The predominant coupling in aHCs and eHCs was between theta/alpha phase and gamma power. In CDCs such coupling was lost and replaced by alpha oscillations coupling to delta/theta phase. Thus, alpha/theta oscillations synchronize high-frequency gamma activity only in hearing-experienced cats. The absence of induced alpha and theta oscillations contributes to the loss of induced gamma power in CDCs, thereby signifying impaired local network activity.

1. Introduction

Cochlear stimulation activates the auditory cortex through thalamic inputs, and subsequently, the auditory cortical areas interact via corticocortical connections to analyze and represent the sensory input, and integrate it into the ongoing cortical processing. These activations are reflected in cortical local field potentials (LFPs) in the form of stimulus phase-locked and non-phased-locked oscillations (Singer, 2011; Buzsaki, 2006). Provided that oscillations occur in a synchronized manner in different neurons, the downstream activation of neuronal targets becomes effective and provides a way to functionally "bind" distributed neurons into functional networks or assemblies. Synchronization of oscillatory processes thus allows the representation of sensory features of an object in a distributed manner across different and distant cortical regions (Engel et al., 2001). Low-frequency oscillations are especially suited to synchronize distant cortical areas by accommodating longer conduction time between distant structures (Buzsaki, 2006).

In the auditory cortex, oscillatory activity has been described previously (MacDonald and Barth, 1995; Sukov and Barth, 2001; Lakatos et al., 2005; Harris et al., 2011; Giraud and Poeppel, 2012). Signatures of different auditory processes were related to oscillatory processes, including stimulus detection (Mercier et al., 2015; van de

* Corresponding author.
E-mail address: prasandhya.a.yusuf@ui.ac.id (P.A. Yusuf).

https://doi.org/10.1016/j.heares.2024.109032
Received 15 January 2024; Received in revised form 30 April 2024; Accepted 13 May 2024
Available online 17 May 2024

Nieuwenhuijzen et al., 2016), listening effort (Dimitrijevic et al., 2017), auditory sensory and cognitive load (Brilliant et al., 2024), and auditory attention (Wöstmann et al., 2017). In the development of auditory cortex, additionally to a shift of oscillatory activity towards higher frequencies with postnatal age (Uhlhaas et al., 2009; Kaminska et al., 2017), also a particular pattern of development is observed in high-frequency oscillations that peak in adolescence (Cho et al., 2015). Early onset deafness affects these oscillations (Yusuf et al., 2017), demonstrating their developmental plasticity.

Sensory responses can be differentiated into evoked (stimulus-phase-locked) and induced (not stimulus-phase-locked) responses (Tallon--Baudry et al., 1996; Chen et al., 2012; Yusuf et al., 2017). While evoked activity is dominated by sensory input, induced oscillation can integrate the sensory input into ongoing cortical processing that is not synchronous with the stimulus presentation. Ongoing cortical processing, integrating corticocortical influences (including top-down inputs) into sensory processing, is thus reflected mainly in induced responses. Even brief (few millisecond duration) auditory stimuli induce activity in the primary auditory cortex that outlasts 600 ms and comprises of both low- and high-frequency oscillations (Yusuf et al., 2017). The activity after 100 ms post-stimulus in such conditions contains mainly induced oscillations (ibid.) and is considered a consequence of corticocortical (as opposed to bottom-up thalamocortical) processing (Siegel et al., 2012).

Our previous work studied the effects of auditory deprivation during development. We used congenitally deaf cats (CDCs) that combine inherited deafness with total absence of hearing experience from birth (Kral and Lomber, 2015). Using cochlear implant (CI) stimulation, the function of the auditory system can be directly compared between animals with and without previous hearing experience. Thereby, it has been demonstrated that congenital deafness extensively affects the development of the auditory cortex, cortical synapses, and increases the amount of developmental synaptic pruning (Kral et al., 2005). By that, congenital auditory deprivation leads to numerous functional deficits in the auditory cortex and to developmental critical periods (review in Kral and Sharma, 2012; Kral et al., 2019). Structural connectivity (i.e. fiber tracts connecting brain regions) is reorganized in strength in CDCs, but it includes only a few abnormal (ectopic) connections (Barone et al., 2013; Butler et al., 2017). While structural connectivity is a precondition for functional connectivity, functional connectivity additionally includes synaptic number, synaptic efficacies and functional postsynaptic properties that are not reflected in structural connectivity. Therefore, structural and functional connectivity correlate only weakly (Suarez et al., 2020; Avena-Koenigsberger et al., 2018).

We previously documented extensive deficits in functional connectivity in CDCs: congenital deafness nearly eliminated induced activity in the feline auditory cortex (Yusuf et al., 2017) and massively reduced top-down interactions between secondary and primary auditory cortex, conveyed by alpha and partly beta oscillations (Yusuf et al., 2021, 2022). However, in stark contrast to deficient sensory-related functional connectivity, interareal functional connectivity in spontaneous activity was either stronger (in supragranular layers) or similar (in infragranular layers) in congenitally deaf cats compared to hearing-experienced cats (Yusuf et al., 2021; 2022). The deficits in the corticocortical couplings were thus specifically related to the processing of the auditory stimulus. The deficits likely included two components: (i) a sensory component that depolarizes the neurons in the given time window and facilitates corticocortical interactions, and (ii) active corticocortical connections that synchronize the neurons between different cortical areas.

Oscillatory processes often occur in a nested sequence where high-frequency oscillations appear during a preferred phase of low-frequency oscillations (Fries, 2005; Fries et al., 2007). Here, low-frequency oscillations reflect neuronal excitability in large-scale networks and the high-frequency oscillations reflect the activation of the local subnetwork (Canolty and Knight, 2010). Such a nested sequence of different oscillatory frequencies has been observed in the corticohippocampal system (Lisman and Jensen, 2013; Buzsáki and Wang, 2012), sensorimotor system (von Nicolai et al., 2014), visual system (Fiebelkorn et al., 2013) and prefrontal cortex (Tsunada et al., 2011). Low-frequency brain rhythms are often entrained by external events and cognitive processes (Schroeder and Lakatos, 2009). Phase entrainment to low-frequency oscillations may then propagate through the network via long-range connections (Hyafil et al., 2015), since the long phase duration allows for sufficiently coincident excitation despite conduction delays. Since low-frequency oscillations often provide the necessary depolarization that allows high-frequency activity, a cross-frequency coupling is observed in the recordings. Different modes of sensory processing affect this cross-frequency coupling (review in Canolty and Knight, 2010; Hyafil et al., 2015). How sensory deprivation affects these relations, both in ongoing and stimulus-related connectivity, has not been assessed so far. This is particularly important given that auditory deprivation extensively affects local columnar circuits (Kral et al., 2000; Berger et al., 2017). High-frequency oscillations (in the gamma band) are considered a sign of the activation of such cortical local subnetworks (Canolty and Knight, 2010).

The aim of the present study was to determine whether the loss of induced oscillations at high frequencies in congenital deafness (Yusuf et al., 2017) can be related to the reduced top-down interactions conveyed by alpha oscillations in CDCs (Yusuf et al., 2021) or whether they represent a phenomenon on its own. Significant gamma power coupling to the phase of low-frequency oscillations might explain the loss of gamma oscillations in CDCs by the simple loss of low-frequency activity (alpha, theta). Alternatively, the loss of gamma oscillations may be an additional phenomenon not directly related to low-frequency oscillations. Here we therefore analyzed cross-frequency coupling and quantified (i) cross-frequency phase-amplitude coupling (PAC, i.e. the power of high-frequency oscillations as a function of the phase of low-frequency oscillations) and (ii) the relation of evoked oscillations to induced activity (power-power coupling) in both CDCs and hearing experienced cats. We report here significant cross-frequency couplings in the large majority of recording sites in hearing-experienced cats, predominantly gamma oscillations ($>$ 30 Hz) that coupled to the phase of theta activity (4–7 Hz) and to the phase of alpha (8–15 Hz) activity. In congenital deafness, these disappeared and were replaced by alpha oscillations coupling to delta (0–3 Hz) and theta phase.

2. Methods

The experimental procedures have been described in detail in a previous study (Yusuf et al., 2017) and will be recapitulated here.

2.1. Subjects

Fifteen adult cats, 10 normal hearing cats (HCs), and five congenitally deaf cats (CDCs) were used. The CDCs were selected from a colony of deaf white cats using early screening of hearing status with acoustically-evoked brainstem responses, showing no ABR responses up to 120 dB SPL (Heid et al., 1998). The hearing status of all cats was additionally confirmed at the beginning of the acute experiments. From the 10 normal HCs, in the final (acute) experiments, four were stimulated only acoustically, two were first stimulated acoustically and, in the same experiments further stimulated electrically using a cochlear implant (CI), and the last four were stimulated exclusively using a CI. This resulted in a sample of six electrically-stimulated (electric Hearing-experienced Control, eHC) and six acoustically-stimulated (acoustic Hearing-experienced Control, aHC) data sets. For simplification of the text, eHCs and aHCs will be together called *controls* in what follows.

Electrophonic responses, i.e. responses of hair cells to electrical stimulation of the cochlea, are not present in deaf animals but "contaminate" responses in hearing animals (Sato et al., 2017). To prevent such electrophonic responses in all electrically-stimulated hearing animals, the hair cells (present in HCs but absent in CDCs)

were destroyed pharmacologically by intracochlear application of neomycin into the scala tympani in the same acute experiments (Sato et al., 2016). The adjective "hearing" thus does not refer to the functional status of the cochlea during the experiment, but refers to the developmental and functional state of the central auditory system that has developed under the normal cochlear function before the acute experiment. In the following text we will use the term *auditory stimulus* as a common term for both the acoustic and the electric (CI) stimulation, since both these activate the auditory system.

The experiments were approved by the local state authorities and were performed in compliance with the guidelines of the European Community for the care and use of laboratory animals (European Directive 2010/63/EU) and the German Animal Protection Law.

2.2. Experimental procedures

All animals were initially anaesthetized with ketamine hydrochloride (24.5 mg/kg, Ketavet, Parker-Davis, Germany) and propionyl promazine phosphate (2.1 mg/kg, Combelen, Bayer, Germany) with an additional 0.25 mg atropine i.p.. They were then tracheotomized and artificially ventilated with 50% O_2 and 50% N_2O, with the addition of 0.2–1.5% concentration of isoflurane (Lilly, Germany) to maintain a controlled depth of anesthesia (Kral et al., 1999). End-tidal CO_2 was monitored and maintained below 5%, and the core temperature was kept above 37.5 °C using a homeothermic blanket. The animal's status was further monitored by blood gas concentration measurements, pH, bicarbonate concentration and base excess, glycaemia, and oxygen saturation determined from capillary blood. A modified Ringer's solution containing bicarbonate and plasma expander was infused i.v. (50 ml/kg/day) with 5 μl atropine and additional bicarbonate, depending on the acid-base status. Monitoring and correction of the acid-base balance was performed every 12 h.

The animal's head was fixed in a stereotactic frame (Horsley-Clarke). Both bullae and ear canals were subsequently exposed. To record evoked auditory brainstem responses, a small trephination was drilled at the vertex of the skull and a silver-ball electrode (diameter 1 mm) was attached epidurally. The indifferent electrode used for the recordings was inserted medially into the neck muscles, the animal was further grounded by a subcutaneous electrode.

Hearing status was verified using acoustically-evoked auditory brainstem evoked responses (ABRs) with condensation clicks applied through a calibrated speaker (DT48, Bayer Dynamics, Germany) at levels up to 120 dB SPL. For electrical stimulation, HCs and CDCs were implanted with a CI inserted via the round window. Electrically evoked auditory brainstem response (E-ABR) to single biphasic pulses was recorded and the lowest current levels evoking a brainstem response (E-ABR-threshold currents) were determined. ABRs were preamplified (60 dB, Otoconsult V2 low-impedance amplifier), amplified (40 dB, Otoconsult Amplifier-Filter F1, filters 0.010–10 kHz) and recorded using National Instruments MIO cards. The signals were averaged (200 sweeps, repetition rate 33 Hz, Audiology Lab, Otoconsult, Frankfurt am Main). The absence of acoustically evoked brainstem responses (including wave I, generated within the auditory nerve) to clicks above 120 dB SPL verified complete deafness. All hearing ears were deafened by slow instillation of 300 μl of Neomycin sulfate into the scala tympani (within 5 min.). The Neomycin was left in place for a further 5 min. and subsequently washed out by slow instillation of Ringer's solution. The total absence of auditory evoked brainstem responses verified that the deafening procedure was successful. Deafening was performed around 30 min. before the cochlear implantation in the same acute experiments. None control hearing animals thus had a significant period of deafness before the acute experiments.

For acute electric stimulation through a CI, charge-balanced pulses (200 μs/phase, repetition rate 2 Hz) were applied to the CI (wide bipolar stimulation, stimulation interelectrode distance ~3 mm). Stimulation was performed with optically isolated current sources (CS1, Otoconsult, Germany).

In A1, recordings were at positions showing the largest surface local field potentials (LFPs) determined in surface mapping ("hot spots"; for details, see (Kral et al., 2009, 2013b). A single-shank multielectrode array (NeuroNexus, USA, single shank, 16 contacts, spacing 150 μm, 177 μm^2 contact area, electrode array length 2400 μm, impedance ~1–2 MΩ) was used to penetrate A1 perpendicularly to the cortical surface to 2400 μm depth. At least one penetration in each animal was marked by a fluorescent dye (DiI, 1,1′-dioctadecyl-3,3,3′,3′-tetramethylindocarbocyanine perchlorate; Invitrogen) to allow histological reconstruction of the penetration track. For all recordings, the cortex was stabilized by a modified Davies chamber (details in Tillein et al., 2010).

2.3. Stimulation and recording

Ears contralateral to the studied cortical hemisphere were electrically stimulated by patterns of three biphasic electric charge-balanced pulses (200 μs/phase, 500 Hz repetition rate) presented through CIs, or acoustically stimulated by three condensation clicks (50 μs duration, 500 Hz repetition rate) presented through loudspeakers (repetition rate 500 pps, stimulus duration 4.4 ms). The stimulus presentation rate was 1/1537 ms (~0.65 Hz) with 30 stimulus repetitions. Stimulation level was increased in 10 dB (acoustic) or 1–2 dB (electric) steps. Stimulation intensities were from at least 10 dB (acoustic) or 1 dB (electric) below threshold to at least 40 dB (acoustic) or 9 dB (electric) above the acoustic and electric ABR threshold, respectively. Recordings were analyzed at defined supra-threshold levels, i.e. 6 dB above the E-ABR threshold of the given stimulus in electric stimulation and 40 dB above the ABR threshold with acoustic stimulation (for details, see Yusuf et al., 2017).

Signals were amplified by a 64-channel Cheetah amplifier (Neuralynx, Bozeman, MO, USA) with a gain of 5000 and open filters (1–9000 Hz), fed to a multifunctional data acquisition card (NI PCIe 6259, National Instruments, USA), 16-bit A/D converted at a sampling rate of 25 kHz per channel and stored on a computer. Here, we concentrated on recordings in the most responsive region of field A1, where in total 23 penetrations in aHC, 23 penetrations in eHC, and 9 penetrations in CDC were analyzed.

2.4. Data analysis in time domain

Offline data analyses were performed using the FieldTrip toolbox (Oostenveld et al., 2011) and custom-made Matlab scripts (Matlab, Mathworks). Recordings with technical artifacts or periods with repeated spontaneous bursting were excluded from the analysis (for details, see (Yusuf et al., 2017).

LFP signals were first resampled (1 kHz sampling rate) and were baseline corrected in the time domain (to eliminate overall baseline drift and to minimize edge artifacts in time-frequency computation, see Herrmann et al., 2014).

2.5. Time domain analysis

All data processing and analyses mentioned in this section were performed offline using the FieldTrip toolbox (Oostenveld et al., 2011) and custom-made Matlab scripts (MATLAB, Mathworks). Noisy recordings, signals with burst-suppression, and channels with artifacts before the analyses were excluded (for details, see Yusuf et al., 2017).

Discrete Fourier transform (DFT) filters at 50 and 100 Hz were applied to remove power line artifacts. The DFT fits a sinusoid of the corresponding frequency to the signal and subtracts it subsequently, operating similar to a notch filter but without the signal distortion introduced by a notch filter. Subsequently, the detrend (demean) procedure was applied to the LFP signals to remove any possible DC shift on the recordings. We reduced the far-field components in A1 by subtracting every two neighboring channels within an electrode shank from each other, yielding the bipolar derivation LFP (**b-LFP**) signals. We

removed the transient evoked components by subtracting the time domain averaged signal from each trial, allowing the analysis of the non-phase-locked part only.

2.6. Time-frequency analysis of b-LFPs

The time-frequency domain was calculated using complex wavelet transformation (Morlet wavelets, $m = 6$, 1 ms steps, frequencies 5 - 119 Hz with 2 Hz linear steps). Time-frequency regions affected by the edge (border) artifacts were excluded from the analysis. Frequency bands were later separated into delta (1–3 Hz), theta (4–7 Hz), alpha (8–15 Hz), beta (16–30 Hz), low gamma (31–60 Hz), high gamma (61–120 Hz).

The phase-locking factor (PLF, Tallon-Baudry et al., 1996) was computed before DFT filtering to preserve the phase information. The complex time-frequency values for each trial were first normalized (vector length=1), summed (vector addition) over trials, and then the absolute value was taken. We used the PLF critical value as a statistical threshold (Cohen, 2014):

$$PLF_{crit} = \sqrt{\frac{-\ln(p)}{N}} \quad (1)$$

where p denotes the p-value and N is the number of trials. With $N = 30$ and $p = 0.01$, consequently, PLF_{crit} for our setup was 0.3918.

Channels were considered responding if the early-latency PLF value (0–100 ms post-stimulus) exceeded mean + 4 times SD of baseline activity in any consecutive 20 ms time window at any frequency.

2.7. Spectrum analyses using matching pursuit

To capture the highly dynamic cortical activities containing both oscillatory and transient components, a time-frequency transform called the Matching Pursuit (MP) algorithm was used to decompose the signal and to reveal the evoked and induced responses (Chandran et al., 2016). The method distributes the energy of the signal over the two independent variables time and frequency (thus called time-frequency distribution, TFD), including the low-frequency components without compromising resolution in both domains (Mallat and Zhang, 1993). This method is advantageous for accessing the low frequencies from briefer trial time windows of the recorded LFP data due to its superior time-frequency precision (Ray and Maunsell, 2011). Each b-LFP trial was then transformed into the time-frequency domain. To exclude the influence of outliers in averaging we used the median averaging (Yusuf et al., 2017).

To represent the **TFD** relative to the pre-stimulus period (baseline), scaling the power data to standard deviation units of the baseline period (z-transform) was chosen (Eq. (2)):

$$z_{values} = \frac{activity - mean(baseline)}{SD(baseline)} \quad (2)$$

This transform corrects the logarithmic decay power and transforms power data to be comparable across frequencies, electrodes, and animals. The results are in z-values which more straightforwardly show significant responses (Cohen, 2014). Significant TFD is denoted by a black contour in the figures, determined using the Bonferroni-corrected significance threshold of $p < 0.05$ divided by the number of time–frequency bins.

The total power TFD was computed from the TFDs of the original b-LFPs. Induced power was determined by subtracting the time-average b-LFP from each trial before TFD computation. Subsequently, we normalized both total and induced TFDs relative to the baseline period (−400 to −100 ms pre-stimulus) using the z-transform. Additionally, the (baseline-normalized) evoked TFD was obtained by subtracting the baseline-normalized induced TFD from the baseline-normalized total TFD. The evoked TFD represents the phase-locked component while induced TFD represents the non-phase-locked component, both were expressed in the same unit (z-score).

2.8. Cross-frequency coupling

Cross-frequency coupling characterizes the interaction between brain waves of different frequencies. Here, we assessed 1) phase-amplitude coupling (PAC), i.e. correlation between phase of low frequencies and amplitude of high frequencies, and 2) power-power correlation, i.e. correlation between low frequency evoked with high frequency induced responses. Both were analyzed within the frequencies recorded at the same cortical recording site. Modulation index was used as introduced by Tort and team (Tort et al., 2010). Modulation index operates by discretizing the time series of phase angles (associated with frequency) into 18 phase bins and then determining the average power of the modulated frequency for each bin. Consequently, the phase–amplitude histogram displays a non-uniform distribution of power across the phase bins. Here we used 20 logarithmic steps, each for phase frequencies (from 2 to 32 Hz, Morlet wavelet $m = 6$) and for amplitude frequencies (from 8 to 128 Hz, Morlet wavelet $m = 4$).

We additionally included the debiased PAC (dPAC) method as introduced by van Driel as a comparison (van Driel et al., 2015). This method modifies the phase-amplitude coupling (PAC) method (Canolty et al., 2006) to encounter the possible over- and underestimations, Type-II errors, and uninterpretable statistical outcomes (van Driel et al., 2015). Both cross-frequency coupling methods were computed from the whole-time b-LFP signals (pre- and post-stimulus time window).

To assess the statistical significance of the cross-frequency coupling we shuffled the power time series relative to the phase angle time series ($N = 500$ permutations), yielding z-values. Since the relationship between phase and power is rendered random through this shuffling, it is expected to create a null distribution of the modulation index and dPAC values. This null distribution is generated under the assumption of a uniform distribution of power across phase bins, forming the basis for the null hypothesis. This permutation testing will also effectively tackle the phase clustering bias (van Driel et al., 2015). Significant cross-frequency couplings denoted by the black contours were determined using the Bonferroni-corrected significance threshold of $p < 0.05$ divided by the number of frequency–frequency bins. The grand mean was constructed only from significant cross-frequency coupling for each animal group.

The power-power correlation between evoked theta responses and induced alpha, beta, low gamma, and high gamma responses was computed using Spearman's rank correlation coefficient to assess the monotonic relationship.

3. Results

The present data rest on intracortical recordings using 16-site multielectrode arrays obtained within the region of strongest responses (hot-spot 1, Kral et al., 2009) in the primary auditory field A1, as determined in a functional mapping procedure (for details, see Kral et al., 2009, 2013b). The penetrations were perpendicular to the cortical surface and covered all cortical layers. Here we used only significantly auditorily-responsive sites (i.e. sites responsive to acoustic stimulation in aHCs and responsive to electric stimulation in eHCs and CDCs) following bipolar derivation of the recordings. Based on the criterion of responsiveness (see methods) we compared 284 auditory responsive sites in aHCs, 237 responsive sites in eHCs and 114 responsive sites in CDCs.

A typical auditory response in hearing cats included a strongly phase-locked response within the first 150 ms after stimulus onset, and an oscillation afterwards representing ongoing oscillations and oscillatory transients (Fig. 1). Unit response (Fig. 1A) and local field potential (Fig. 1B,C) correspond to each other, showing an early (0–150 ms) phase-locked response (at the exact time point) and a late (>150 ms)

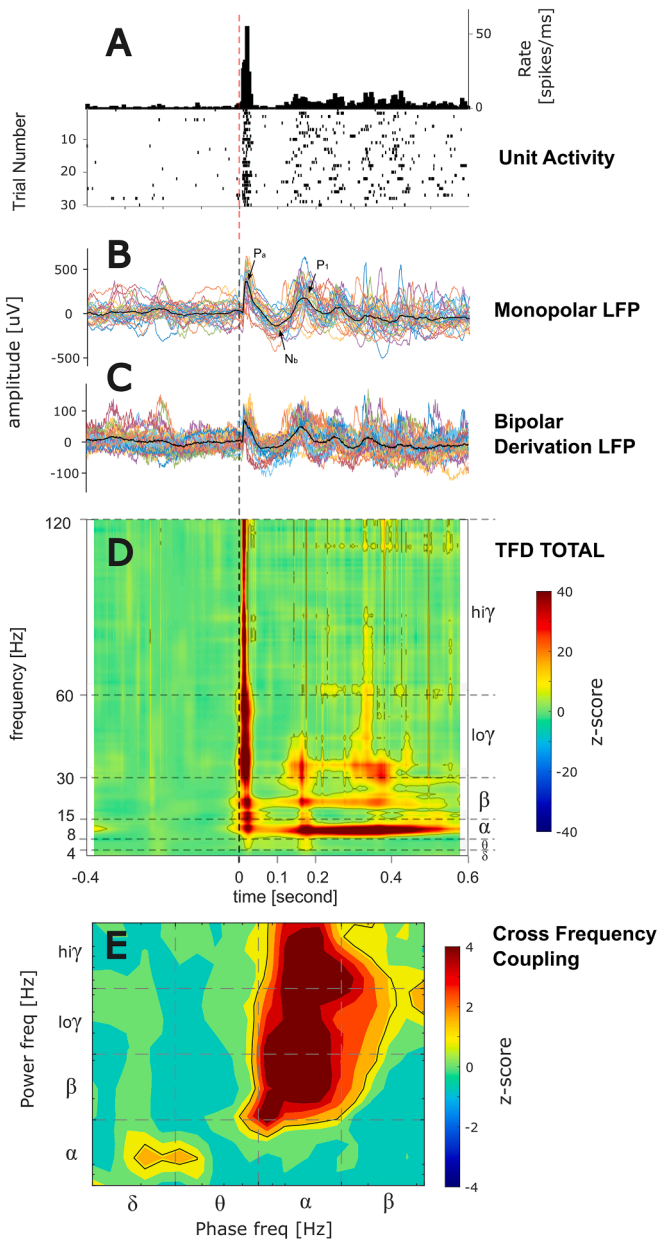

Fig. 1. Example of a single recording in an acoustic control (aHC). Stimulation was with a train of 3 condensation clicks (50 μs duration, 500 Hz repetition rate, stimulus duration < 6 ms). **(A)** Peristimulus time histogram and raster plot of unit activity. **(B)** Monopolar local field potential (LFP) of the same recording site, colored lines represent 30 trials, thick black line is the average, dashed line represents the time of stimulus presentation. **(C)** Same as B for bipolar derivation local field potential (b-LFP). **(D)** Time Frequency Distribution (TFD) calculated for b-LFP from C by matching pursuit algorithm, shown in z-score relative to the pre-stimulus baseline. The transient response covering all frequencies from theta to high gamma band starts ca. 10–12 ms after the stimulus onset, followed by long-lasting alpha and beta oscillations and gamma transients. Black contours represent significant TFD z-scores after Bonferroni correction for multiple comparisons. **(E)** Phase-amplitude cross frequency coupling, presented in z-score and shown in log-log plot, computed by Mutual Index method with 500 shuffled permutations. Black contours represent significant cross-frequency coupling z-scores with Bonferroni correction. The result demonstrates significant alpha-beta and alpha-gamma PAC.

non-phase-locked response (jittered in time). Interestingly, there was an increase in ongoing firing rate after ~150 ms post stimulus that corresponded to highly-variable local field potentials at these latencies. The matching pursuit (MP) algorithm for time-frequency analysis identified an early broadband response transient and a long-latency ongoing oscillation in the alpha range over nearly 500 ms (Fig. 1D). Parallel to the alpha range oscillations there was beta and gamma activity, whereas the beta and gamma activity was modulated, peaked before 200 and again before 400 ms post stimulus. Cross-frequency coupling revealed a corresponding relation of beta and gamma power to the alpha phase (Fig. 1E).

In what follows, we refer to the cross-frequency coupling in sense of phase-amplitude coupling (PAC), i.e. when referring to alpha-gamma coupling we mean that the phase of alpha oscillations was coupled to the power of gamma oscillations. In this sense the gamma oscillations were synchronized by the alpha phase.

To further elaborate the time-frequency representation statistically, we pooled all data in a grand mean. Since previous studies differentiated the response into a phased-locked **evoked** response, and the non-phased-locked **induced** response (for details see Yusuf et al., 2017), we computed the means for evoked and induced power separately. The grand mean results documented that evoked power was limited to the early onset response (Fig. 2A-C, up to ~ 150 ms, compare Yusuf et al., 2017). There was an additional mean increase in evoked theta power in aHCs lasting 200–300 ms after stimulus onset (white arrow in Fig. 2A-B) not resolved by the analysis methods previously. This was possible by the use of the MP algorithm that has minimal time-frequency tradeoff (see discussion).

In the evoked activity of the eHC group (Fig. 2B), power similarly increased through all bands in the time window 0–50 ms post-stimulus, and included also a theta band response and a beta band response lasting 200–300 ms (white and black arrow in Fig. 2B). This suggests that with high time-frequency precision of the MP algorithm, a structured low frequency evoked response is detectable in both control groups, and that even an unfamiliar and artificial stimulus, a cochlear implant stimulus, did not reduce this response in eHCs.

Concordantly with previous observations using wavelet analyses, the CDCs showed a strong evoked activity in A1, however, the MP analysis additionally revealed the absence of the evoked theta observed in controls (Fig. 2C). We performed a cluster-based permutation test to identify significant differences between the animal groups (Fig. 2D,E). Evoked theta activity was observed in both aHC and eHC, and was significantly larger in eHCs compared to CDCs (Fig. 2E). This demonstrates that the overall oscillatory response is more restricted to higher frequencies in CDCs.

The time-frequency distributions of induced power (Fig. 2F-H) revealed a reduction of induced activity throughout all frequency bands and a briefer response in CDCs, as previously reported using wavelet analysis (Yusuf et al., 2017), with significant loss of induced alpha, beta and gamma band responses in CDC (Fig 2J). Induced activity was mainly observed in the late time window (> 150 ms post stimulus), with some additional component in the early onset response.

Subsequently, we compared ongoing and stimulus-related power changes. A typical exponential decay with increasing frequency was observable when analyzing the overall ongoing power as a function of frequency (Fig. 3A), demonstrating highest power in low-frequency activity. This was the case for both baseline and response. The ongoing activity in A1 was highest in hearing animals with intact cochleae (aHCs) (Yusuf et al., 2017). After the destruction of hair cells (in eHCs), the power in all frequencies dropped below the level of aHCs, suggesting that ongoing synaptic activity of hair cells provided significant drive to cortical neurons. Deafness partly compensated this in the central auditory system, leading to significantly higher absolute power in CDCs than in eHCs in theta to low gamma bands.

Next, we quantified the frequency changes caused by the auditory stimulation by expressing poststimulus activity in z-scores of

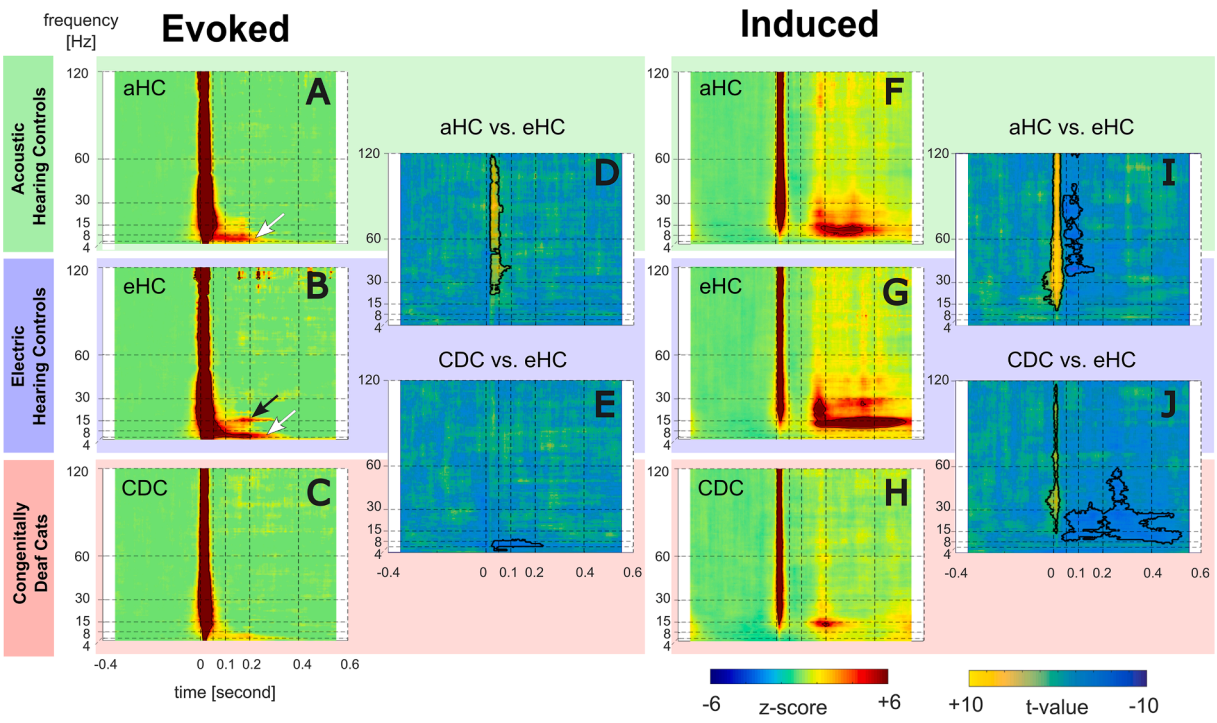

Fig. 2. Time Frequency Distributions (TFDs) grand mean from b-LFP. **(A-C)** TFD of Evoked responses for (A) acoustically stimulated controls (aHC), (B) electrically stimulated controls (eHC), and (C) congenitally deaf cats (CDC). TFDs are presented in z-score baseline. **(D-E)** Non-parametric cluster-based permutation statistics for comparison between: (D) acoustic controls and electric controls and (E) CDCs and electric controls. Statistics were computed with 1000 permutations, cluster alpha threshold 1%, two-tail significant a-value = 0.5%. Data are shown in t-values, significant regions are outlined by black lines. **(F-J)** same as A-E for TFD Induced responses. White arrow denotes the evoked theta response and the black arrow the evoked beta response observed with matching pursuit but not in previous analyses.

prestimulus activity. We concentrated on the significant difference between controls and CDCs, which was found in the late response window (> 150 ms, Fig. 2J). While ongoing activity showed higher power in alpha and beta bands of CDCs than eHCs, neither the total nor the induced auditory responses of CDCs showed significant power increase in this band following the electric (CI) stimulus (Fig. 3B,C). There was a much larger power increase in both controls in these bands (Fig. 3B,C). Comparing the late response window, evoked activity was reduced in theta in CDCs (Fig. 3D), and through all bands except theta in induced activity (Fig. 3E). The absence of the effects in induced theta is due to the lack of the auditory stimulus effect (Fig. 3C). When combining ongoing activity and stimulus-related activity, theta activity is a very prominent component of ongoing activity (Fig. 3A), yet in stimulus-related activity it is only affected (increased) in the evoked (in HCs) but not in the induced activity (Figs. 2,3B).

We subsequently systematically analyzed the cross-frequency coupling in cortical local field potentials. We found such couplings consistently in > 70% of responsive recordings sites in all three group of animals (78% in aHCs, 75% in eHCs and 79% in CDCs). In aHCs (Fig. 4A, D), most abundant coupling was between theta and higher frequencies, particularly theta and gamma and alpha and gamma. However, high frequency oscillations (beta and gamma) coupled also to the phase of alpha band and low-frequency gamma also to the phase of the beta band. Particularly the coupling of gamma-oscillations was well reproducible, providing a statistically significant deviation from 0 in the grand mean. This highlights the link between low-frequency oscillation phase and gamma amplitude.

In the eHC group (Fig. 4B,E), the patterns were similar to the aHC group; however, they had a smaller significant area in the grand means, suggesting more variability in the exact frequencies with cross-frequency coupling (N.B.: the number of recording sites with significant cross-frequency coupling was similar between the groups). In eHC we observed similar alpha-gamma PAC as in aHC, suggesting that the artificial and novel electric stimulus does not impair the estimation of cross-frequency couplings but reduces the between-site reproducibility.

In the CDCs (Fig. 4C,F) the grand mean results were distinct from both controls. There was significant delta-alpha and theta-alpha PAC not observable in controls, but few reproducible alpha-gamma PAC with no statistical significance. This demonstrates a shaping influence of experience on cross-frequency coupling and suggests a key role of alpha oscillations in deprivation-caused deficits in the auditory cortex.

Finally, we were interested in the relation of the evoked theta activity to induced oscillations, considering that the evoked response might constitute a key excitatory event providing a precondition for induced oscillatory activity. We therefore studied the relation of evoked theta power to the induced power in all bands using power-to-power cross-frequency couplings (Fig. 5). In both control groups, there was a significant monotonic correlation of the evoked theta power to the induced activity, suggesting that the phenomena indeed co-occur and that high theta power is predictive of more induced activity. This suggests that the evoked response provides a window of opportunity for corticocortical interactions that include more power if there is an evoked response in the theta band. However, the theta power variation explained at maximum of 18.9% of the variability in the alpha band and even less in the other bands in eHCs, and even less in aHCs. In CDCs the correlations were in all cases not significant.

4. Discussion

Cross-frequency coupling was found similarly often (at >70% recording positions) in congenitally deaf cats as in controls. However, the coupled frequencies changed in congenital deafness. In both electrically and acoustically-stimulated controls, gamma oscillations showed a significant coupling to alpha and theta phase (Fig. 4). Unlike the alpha oscillations that were stimulus-related, the cross-frequency coupling of theta phase to gamma power was mainly related to

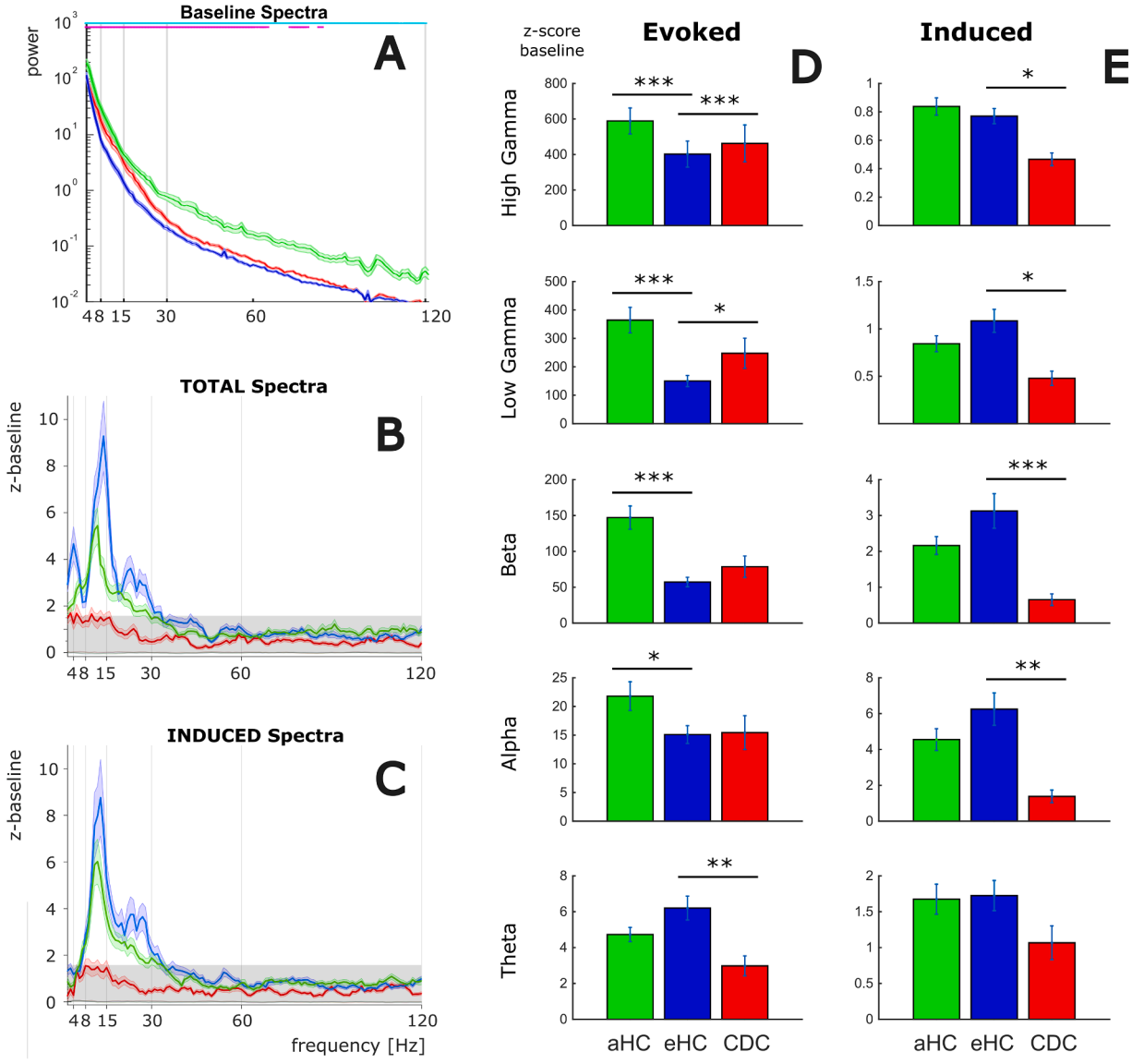

Fig. 3. Spectra of the recordings in A1. **(A)** Overall power of the recorded signal in the pre-stimulus baseline for three animal groups, shown as mean (thick colored lines) and standard error of the means (shaded colors). Shown are acoustically stimulated controls / hearing animals with intact cochlea (aHC, green), electrically stimulated controls / hearing acutely deafened animals (eHC, blue), and congenitally deaf animals (CDC, red). Magenta line above the plot designates significant difference between eHCs and CDCs, cyan line between aHCs and eHCs (two-tailed Wilcoxon rank-sum test, FDR corrected $q < 0.05$). **(B)** TFD total spectra in response to the stimulus (150–600 ms window, excluding the onset response) in z-score relative to baseline, as obtained using MP algorithm. **(C)** TFD induced spectra (150–600 ms window) in z-score, as obtained using MP algorithm. Gray shading in B-C denotes zscore with $p > 0.05$ **(D)** Evoked Response frequency band-wise bar plot comparison between acoustic vs. electric-stimulated controls and congenitally deaf vs. electric-stimulated controls. Frequency bands were separated into theta (4–7 Hz), alpha (8–15 Hz), beta (16–30 Hz), low gamma (31–60 Hz), high gamma (61–120 Hz). **(E)** same as D for Induced Response. Comparing between hearing (green for aHC, blue for eHC) and deaf (red) groups, there was substantial effect of the stimulus on the induced alpha-beta-gamma responses, however in evoked oscillations a significant difference was only present in gamma and theta band. $*p < 0.05$; $**p < 0.01$; $***p < 0.001$.

ongoing (not stimulus-related) theta oscillations.

While in the baseline spectra no loss of oscillatory power was observed (in neither band) in CDCs compared to eHCs (Fig. 3A), high-frequency gamma oscillations were not coupled to theta and alpha phase in CDCs (Fig. 4C,F). Instead, alpha oscillations were coupled to the phase of the low-frequency delta and theta phase in CDCs. The findings underscore (i) the role of induced alpha oscillations in the generation of stimulus-related gamma responses in controls, with ongoing theta contributing, and (ii) the key developmental role of auditory experience on these oscillations.

Network changes including reduced long-distance spike-field coherence were previously demonstrated in CDCs compared to HCs (Yusuf et al., 2022), together with reduced top-down interareal coupling, normally conveyed by alpha oscillations (Yusuf et al., 2021). This suggests that the effects of deafness on alpha oscillations may be a common link between numerous deficits of the auditorily-naïve (deaf) auditory cortex.

4.1. *Matching pursuit analysis*

Methodologically, the present study document that Matching pursuit (MP) is a method that provides a high level of specificity in the time-frequency domain (Mallat and Zhang, 1993; Schiecke et al., 2015). MP is a form of time-frequency analysis that calculates the time-dependent spectral density of the signal using a combination of Gabor functions (called atoms) localized in time and frequency,

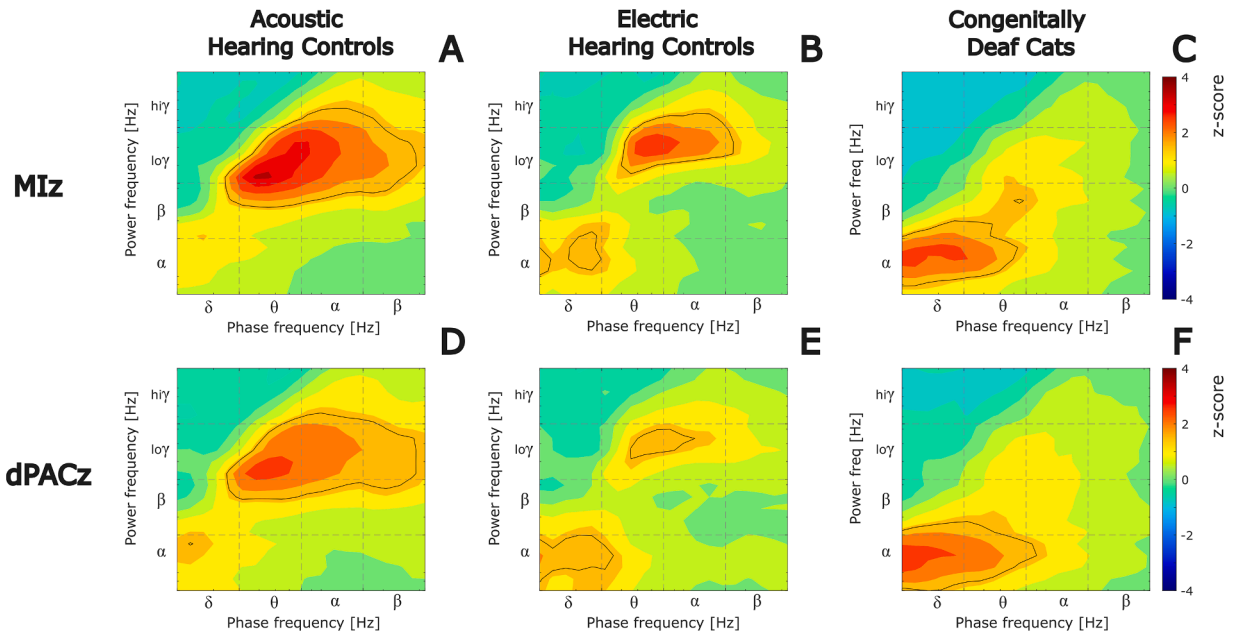

Fig. 4. Cross-frequency phase-amplitude coupling grand mean for the three animal groups. (A,D) hearing, acoustically stimulated animals, (B,E) hearing, electrically stimulated animals, (C,F) congenitally deaf animals. CFCs were computed using Modulation Index (MI, A-C) and debiased phase-amplitude coupling (dPAC, D-F). All data were presented as z-scores and shown in log-log plots, black lines mark significant CFCs ($p < 0.05$, 500 permutation statistics with Bonferroni correction). While both hearing groups show a prominent theta-gamma and alpha-gamma coupling, the congenitally deaf group shows more robust delta-alpha and theta-alpha coupling.

approximating the spectral density changes of the signal over time (thus calculating in two rather than one dimension, as in Fast Fourier Transformation). The identified atom is shifted and scaled to best fit the signal, and then the remaining signal undergoes iteratively the same procedure for the next atom until it is completely described by the algorithm in time and frequency (Chandran et al., 2016). It approaches the highest possible temporal vs. frequency resolution, with the advantage of no trade-off between the resolution in time and in frequency. For the present goal, the method represented a major advantage due to its exquisite time-frequency precision. It allowed studying the effects of hearing loss on theta activity that were not resolved previously (Yusuf et al., 2017). On the other hand, the observed effects of congenital deafness were in other frequency bands similar to those described earlier (human: Morillon et al., 2012; hearing and congenitally deaf cats: Yusuf et al., 2017). This correspondence demonstrates the robustness of the MP approach.

There are, however, also disadvantages compared to Fast Fourier Transformation or wavelet analysis: the slower computation process, and the results that cannot be directly used for phase-based functional connectivity analysis. The advantage of high spectrotemporal precision of the present results provides also a complication for the statistical analysis. While cluster-based methods of statistical analysis (Groppe et al., 2011a, 2011b) compensate for the size of the significant "islands" in wavelet-computed time-frequency representation, the high time-frequency precision might reduce the power of the statistics in MP-computed time-frequency distribution due to natural and individual fluctuations of the exact time and frequency at which responses appear. This may have reduced the sensitivity of the statistics, especially for transient responses as observed in the gamma range.

4.2. Cross-frequency coupling in controls

The present results in hearing cats document cross-frequency coupling of high frequencies (beta and gamma) to low frequencies (alpha and theta) phase in the "hearing" auditory cortex, suggesting a nested oscillatory sequence similar to the corticohippocampal system (Lisman and Jensen, 2013; Buzsáki and Wang, 2012), sensorimotor system (von Nicolai et al., 2014), visual system (Fiebelkorn et al., 2013) and prefrontal cortex (Tsunada et al., 2011). Gamma-band activity was linked to alpha and theta phase in the present study. The pre-stimulus phase of alpha and theta activity is crucial for discriminative behavior and learning (Michael et al., 2023; Köster et al., 2019). Low-frequency oscillations depolarize the neurons in a one-half period of the oscillation. By that, in a one-half period, they decrease the threshold for high-frequency oscillations. High-frequency oscillations are then coupled to the phase of low-frequency oscillations. It has been previously reported in other sensory systems and related to long-range interactions functionally coupled to local interactions (Fries, 2005; Fries et al., 2007; García-Rosales et al., 2018; Duprez et al., 2020). This pattern of cross-frequency coupling is considered an oscillatory signature of the adequate activation of local neuronal circuits and was observed here only in hearing-competent animals. More pronounced cross-frequency coupling in acoustic as compared to electric stimulation underscores the role of stimulus familiarity in cross-frequency coupling (Canolty and Knight, 2010). Using human EEG recordings, similar relations were observed during development (Cho et al., 2015). Remarkably, the role of theta activity was different from alpha activity in the present study: while induced alpha power increased by stimulation substantially, stimulus-related theta activity was less prominent and observable only as evoked power increased (in controls, Fig. 2).

4.3. Cross-frequency coupling in CDCs

Cross-frequency coupling in CDCs was not significant between theta/alpha and gamma, but was instead observed between alpha power and theta and delta phase (Fig. 4). Neither delta nor theta power increased after the auditory stimulus in CDCs (Fig. 3B). Thus, it must be the ongoing delta/theta activity, and not activity related to the stimulus, that synchronized the alpha oscillations. Contrary to controls, in CDCs there was no local network activity signified by induced gamma oscillations. The coupling of alpha activity to stimulation-unrelated theta in CDCs would be explicable by a relation to a distant neural structure that

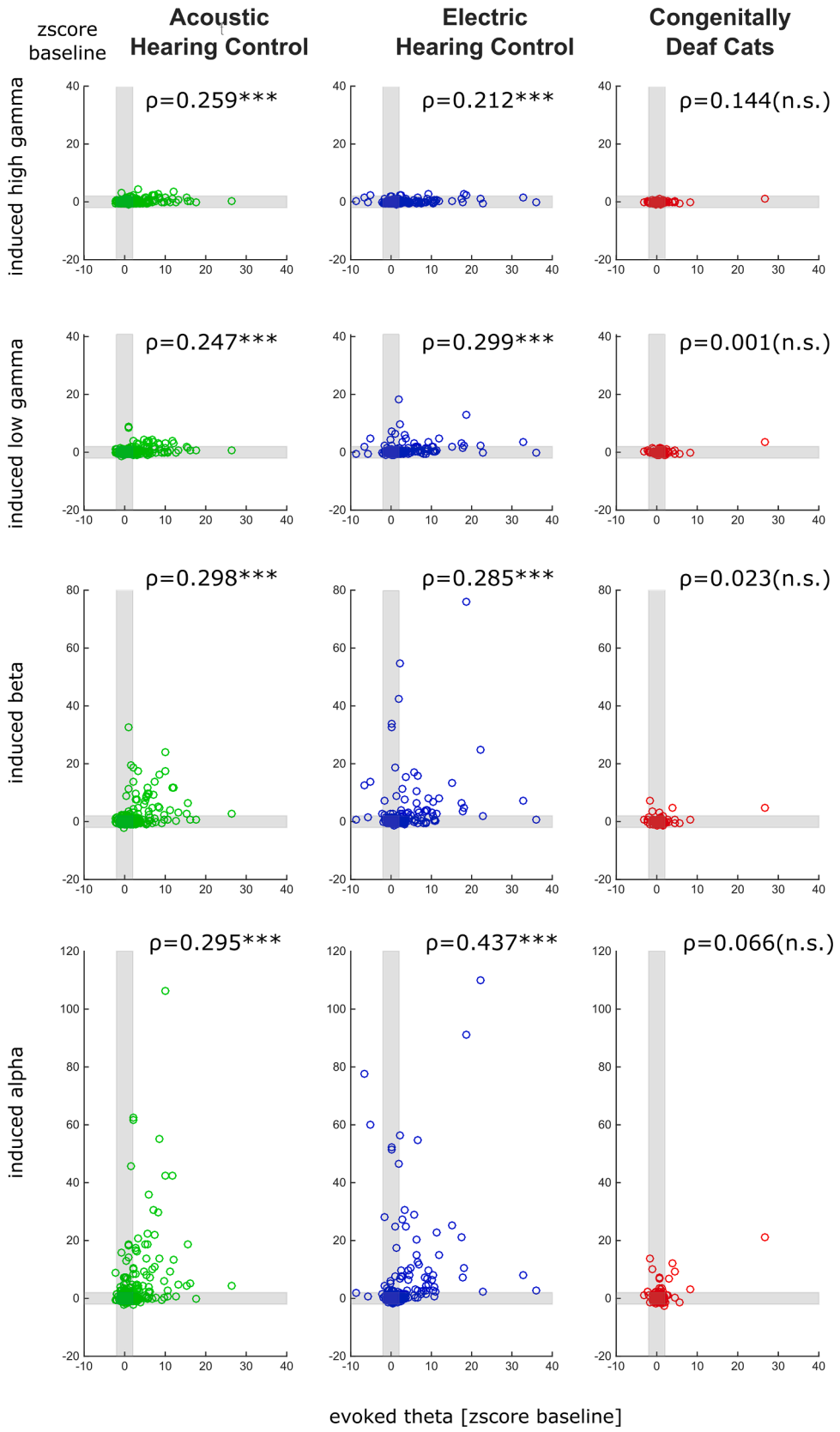

Fig. 5. Power-power correlation between evoked theta responses and induced alpha, beta, low gamma and high gamma responses. ρ values indicate Spearman correlation coefficient, *** $p < 0.001$. Gray shading denotes z-scores with $p > 0.05$.

is not synchronously active with the auditory stimulus, thus a non-auditory function (Kral et al., 2016; Manini et al., 2022; see below). While structural connectivity shows only modest changes in CDCs (Barone et al., 2013; Butler et al., 2017), the present data demonstrate that functional connectivity reorganizes more extensively (comp. review in Kral and Sharma, 2023).

Theta band is interesting since it is crucial, particularly for long-distance synchronization as occurring e.g. between frontal areas and the auditory cortex (García-Rosales et al., 2018; García-Rosales et al., 2020) or cingulate cortex and auditory cortex (Leicht et al., 2021). Auditory-evoked theta, related to the auditory stimulus, was observed in both hearing groups and was significantly smaller in CDCs. Possibly, auditory stimulation fails to recruit these distant structures in CDCs. Evoked theta power was only weakly correlated with induced high-frequency oscillations even in controls. This makes the evoked theta an improbable reason for high-frequency oscillations in controls and therefore an unlikely reason for the loss of induced oscillations in CDCs. It is more likely that the massive loss of induced responses observed in congenital deafness in alpha-to-gamma ranges (Yusuf et al., 2017) is due to reduced cortico-cortical interactions (Tallon-Baudry et al., 1997; David et al., 2006; Widmann et al., 2007; Chen et al., 2012; Sedley et al., 2016; for cochlear implants see Senkowski et al., 2014). Indeed, two previous studies demonstrated loss of inter-areal coupling in the auditory cortex and related this to the absence of top-down interactions conveyed by alpha (and partly beta) oscillations (Yusuf et al., 2022, 2021). Reduced power in auditory-related alpha oscillations would then affect gamma oscillations due to their mutual cross-frequency coupling, as observed here.

These findings are in line with a sight restoration study from congenital blindness, which found weaker evoked theta response in comparison to controls, and late restoration of vision did not compensate for reduced induced alpha activity (Bottari et al., 2016). Taken together the present data are consistent with a loss of mid-range top--down synchronization of the auditory cortex conveyed by alpha oscillations (Yusuf et al., 2022, 2021), and deficits in auditory circuitry leading to weaker responses in the evoked theta range. This results in small evoked P1 responses in the congenitally deaf cat (Kral et al., 2005) and poor long-latency responsiveness in late cochlear-implanted prelingually deaf children (Ponton and Eggermont, 2001; Sharma et al., 2005). Corresponding rearrangement of functional connectivity from within the auditory cortex to other brain systems have been previously reported (review in Kral and Sharma, 2023).

4.4. Evoked theta and trial-averaged LFPs

The loss of evoked theta in CDCs corresponds well to previous studies that documented a P1 (Fig. 1B) component in trial-averaged local field potentials (LFPs) near 100–150 ms post-stimulus in hearing cats (Castro-Alamancos and Connors, 1996a; Kral et al., 2002). At a similar latency, a response was found in unit activity (Fig. 1A, Kral et al., 2006; Castro-Alamancos and Connors, 1996a, 1996b), also in intracellular recordings in awake hearing cats (De Ribaupierre et al., 1972). Layer V neurons are crucial for the presence of the P1 component (Castro-Alamancos and Connors, 1996b). The Nb/P1 complex in some recording sites corresponds in duration to the theta band, explaining its appearance in the grand mean time-frequency representation. The observation of such evoked theta response in controls, but not in CDCs, indeed corresponds to evoked LFP components Nb and P1 as described previously in adult HCs, and their reduced amplitude in adult CDCs (Kral et al., 2002). The role of deep layers is underscored by the dystrophic changes in these layers in CDCs (Berger et al., 2017) together with reduced evoked activity in these layers (Kral et al., 2000). Their near absence in congenitally deaf animals has been rescued by chronic electric stimulation through a cochlear implant within a critical period during development (Kral et al., 2002). The P1 component develops at the age of 2–3 months postnatally, but subsequently disappears during postnatal development in CDCs (Kral et al., 2005). In total, these data on P1 and evoked theta in combination support the conclusion that hearing experience during development plays an important role in preserving the P1 evoked component and evoked theta response.

In the adult age studied here, the evoked theta power explained only a small part of the induced oscillatory activity in controls (Fig. 5). During human development, there is a pronounced change in oscillatory responses. While already in newborns, gamma activity can be observed (Cho et al., 2015), generally juvenile subjects show more low-frequency components and an increase in higher-frequency power is observed during development (Uhlhaas et al., 2009). Provided that such theta (and potentially delta) activity will be evoked by the sensory stimulus in the majority of auditory areas in juvenile age, including primary and secondary areas, it would provide a correlated excitation in the corresponding neurons across cortical areas, and this would provide the possibility for the development of interareal coupling. This is a potential mechanism for the development of auditory cortical areas into a functional unit by binding of the neurons in different areas responding within a similar time window to the same stimulus (Yusuf et al., 2021). During development in hearing animals, the P1 component appears already at 5 weeks postnatally, near the age of the peak in synaptogenesis (Kral et al., 2005). In deaf animals, the P1 declines in amplitude near the end of the critical auditory period in the cat, at around 4 months of age, after the peak in the synaptogenesis was reached and the net synaptic pruning has already been initiated (Kral et al., 2005, 2013a; Kral, 2013). Taken together, this evoked theta transient could provide the window of opportunity for non-auditory couplings to the auditory cortex, e.g. from the cingulate cortex (García-Rosales et al., 2018; García-Rosales et al., 2020), hippocampus through entorhinal cortex (Colgin et al., 2009) and frontal cortical areas (Leicht et al., 2021). Such couplings are key for memory and cognitive processing. Its developmental disappearance in CDCs could delineate a critical period for cochlear implantation.

4.5. Stimulus familiarity vs. absence of experience

In the present study, we compared hearing, acoustically stimulated animals to hearing, electrically stimulated animals. This comparison reveals the role of stimulus familiarity (Handa et al., 2017; Yusuf et al., 2017). The familiar acoustic stimulus provided a different response compared to the unknown and unfamiliar electric stimulus, as it has a representation in the auditory cortex that a completely new, unfamiliar stimulus (such as the electric stimulus in a previously hearing animal) does not have. Higher evoked power was observed with the more familiar acoustic stimulus compared to the novel, unfamiliar electric stimulus in the present study (Fig. 2D,I, Fig. 3D). Also CFC was stronger in acoustic stimulation compared to electric stimulation. Consequently, stimulus familiarity has a significant role in the oscillatory activity related to the stimulus.

5. Conclusion

While in the evoked domain, hearing cats showed theta response that was absent in deaf cats, in the induced domain the theta band played only a minor role in the responses to auditory stimuli in all animal groups. Evoked theta (caused by auditory stimuli) explained less than 19% of the variance in induced responses in hearing cats and thus contributed only to a small extent to higher-frequency induced oscillations. There was significant cross-frequency coupling between low and high-frequency oscillations both under acoustic and artificial electric (cochlear implant) auditory stimulation. Cross-frequency coupling was dominated by alpha-gamma coupling in the auditory cortex of hearing animals, suggesting that alpha oscillations represent a permissive factor for gamma activity. In congenital deafness, it was shifted towards lower frequencies and replaced by delta/theta-alpha coupling, and the induced gamma activity disappeared. The delta and theta activity to

which alpha oscillations were phase-coupled in CDCs were unrelated to the auditory stimulus (neither evoked nor induced). This demonstrates an extensive reorganization of the mutual relations of oscillatory activity in the deaf auditory cortex, with a mediating role of stimulus-related alpha and ongoing theta activity.

Funding

Deutsche Forschungsgemeinschaft (DFG Kr 3370 and Exc 2177); MedEl Comp, Innsbruck, Austria (to J.T.); DAAD – Indonesian German Scholarship Programme (IGSP); PUTI Q2 2020 (NKB-1515/UN2.RST/HKP.05.00/2020) Universitas Indonesia Publication Grant (to PAY).

CRediT authorship contribution statement

Prasandhya A. Yusuf: Writing – review & editing, Writing – original draft, Visualization, Software, Methodology, Funding acquisition, Formal analysis, Conceptualization. **Peter Hubka:** Writing – review & editing, Validation, Supervision, Software, Investigation, Data curation. **Wiebke Konerding:** Writing – review & editing, Investigation. **Rüdiger Land:** Writing – review & editing, Investigation. **Jochen Tillein:** Writing – review & editing, Investigation. **Andrej Kral:** Writing – review & editing, Writing – original draft, Visualization, Supervision, Resources, Methodology, Investigation, Funding acquisition, Conceptualization.

Data availability

Data will be made available on request.

Acknowledgments

We thank Dr. Peter Baumhoff for supporting the experiments and data collection, Karl-Jürgen Kühne and Daniela Kühne for excellent help and assistance in the preparation and during the experiments, including surgery and recordings, as well as preforming the histological tissue processing. We sincerely thank Dr. Supratim Ray (centre for Neuroscience, Indian Institute of Science, Bangalore) for his support with the MATLAB routines for Matching Pursuit.

References

Avena-Koenigsberger, A., Misic, B., Sporns, O., 2018. Communication dynamics in complex brain networks. Nature Reviews Neuroscience 19 (1), 17–33. https://doi.org/10.1038/nrn.2017.149.

Barone, P., Lacassagne, L., Kral, A., 2013. Reorganization of the Connectivity of Cortical Field DZ in Congenitally Deaf Cat. PLoS. One 8 (4), e60093. https://doi.org/10.1371/journal.pone.0060093.

Berger, C., Kühne, D., Scheper, V., Kral, A., 2017. Congenital deafness affects deep layers in primary and secondary auditory cortex. J. Comp. Neurol. 525 (14), 3110–3125. https://doi.org/10.1002/cne.24267.

Bottari, D., Troje, N.F., Ley, P., Hense, M., Kekunnaya, R., Röder, B., 2016. Sight restoration after congenital blindness does not reinstate alpha oscillatory activity in humans. Sci. Rep. 6, 24683. https://doi.org/10.1038/srep24683.

Brilliant, B., Yaar-Soffer, Y., Herrmann, C.S., Henkin, Y., Kral, A., 2024. Theta and alpha oscillatory signatures of auditory sensory and cognitive loads during complex listening. Neuroimage 289, 120546. https://www.sciencedirect.com/science/article/pii/S1053811924000417.

Butler, B.E., Chabot, N., Kral, A., Lomber, S.G., 2017. Origins of thalamic and cortical projections to the posterior auditory field in congenitally deaf cats. Hear. Res. 343, 118–127. https://doi.org/10.1016/j.heares.2016.06.003.

Buzsaki, G., 2006. Rhytms of the Brain. Oxford University Press.

Buzsáki, G., Wang, X.-J., 2012. Mechanisms of gamma oscillations. Annu Rev. Neurosci. 35, 203–225. https://doi.org/10.1146/annurev-neuro-062111-150444.

Canolty, R.T., Edwards, E., Dalal, S.S., Soltani, M., Nagarajan, S.S., Kirsch, H.E., Berger, M.S., Barbaro, N.M., Knight, R.T., 2006. High gamma power is phase-locked to theta oscillations in human neocortex. Science (1979) 313 (5793), 1626–1628. https://science.sciencemag.org/content/sci/313/5793/1626.full.pdf?casa_token=8dQH6iuoBxIAAAAA:BmBEzdWCYDAgsYev9xwvvNdNgU7mN5P-izeoEjg7Jdo9IpMvACkjZB_nI5pxBL9ze0WMhpGIK9RnVtWi.

Canolty, R.T., Knight, R.T., 2010. The functional role of cross-frequency coupling. Trends Cogn. Sci. (Regul. Ed.) 14 (11), 506–515. https://www.ncbi.nlm.nih.gov/pmc/articles/PMC3359652.

Castro-Alamancos, M.A., Connors, B.W., 1996a. Cellular mechanisms of the augmenting response: short-term plasticity in a thalamocortical pathway. J. Neurosci. 16 (23), 7742–7756. PubMed.

Castro-Alamancos, M.A., Connors, B.W., 1996b. Short-term plasticity of a thalamocortical pathway dynamically modulated by behavioral state. Science (1979) 272 (5259), 274–277. PubMed.

Chandran, K.S.S., Mishra, A., Shirhatti, V., Ray, S., 2016. Comparison of Matching Pursuit Algorithm with Other Signal Processing Techniques for Computation of the Time-Frequency Power Spectrum of Brain Signals. J. Neurosci. 36 (12), 3399–3408. https://doi.org/10.1523/JNEUROSCI.3633-15.2016.

Chen, C.-C., Kiebel, S.J., Kilner, J.M., Ward, N.S., Stephan, K.E., Wang, W.-J., Friston, K. J., 2012. A dynamic causal model for evoked and induced responses. Neuroimage 59 (1), 340–348. https://doi.org/10.1016/j.neuroimage.2011.07.066.

Cho, R.Y., Walker, C.P., Polizzotto, N.R., Wozny, T.A., Fissell, C., Chen, C.-M.A., Lewis, D.A., 2015. Development of Sensory Gamma Oscillations and Cross-Frequency Coupling from Childhood to Early Adulthood. Cereb. Cortex. 25 (6), 1509–1518. https://doi.org/10.1093/cercor/bht341.

Cohen, M.X., 2014. Analyzing Neural Time Series Data. MIT Press.

Colgin, L.L., Denninger, T., Fyhn, M., Hafting, T., Bonnevie, T., Jensen, O., Moser, M.-B., Moser, E.I., 2009. Frequency of gamma oscillations routes flow of information in the hippocampus. Nature 462 (7271), 353–357. https://doi.org/10.1038/nature08573.

David, O., Kilner, J.M., Friston, K.J., 2006. Mechanisms of evoked and induced responses in MEG/EEG. Neuroimage 31 (4), 1580–1591. https://doi.org/10.1016/j.neuroimage.2006.02.034.

De Ribaupierre, F., Goldstein, M.H., Yeni-Komshian, G., 1972. Intracellular study of the cat's primary auditory cortex. Brain Res. 48, 185–204. PubMed.

Dimitrijevic, A., Smith, M.L., Kadis, D.S., Moore, D.R., 2017. Cortical Alpha Oscillations Predict Speech Intelligibility. Front. Hum. Neurosci. 11, 88. https://doi.org/10.3389/fnhum.2017.00088.

Duprez, J., Gulbinaite, R., Cohen, M.X., 2020. Midfrontal theta phase coordinates behaviorally relevant brain computations during cognitive control. Neuroimage 207, 116340. https://www.sciencedirect.com/science/article/pii/S1053811919309310.

Engel, A.K., Fries, P., Singer, W., 2001. Dynamic predictions: oscillations and synchrony in top-down processing. Nat. Rev. Neurosci. 2 (10), 704–716. https://doi.org/10.1038/35094565.

Fiebelkorn, I.C., Snyder, A.C., Mercier, M.R., Butler, J.S., Molholm, S., Foxe, J.J., 2013. Cortical cross-frequency coupling predicts perceptual outcomes. Neuroimage 69, 126–137. https://doi.org/10.1016/j.neuroimage.2012.11.021.

Fries, P., 2005. A mechanism for cognitive dynamics: neuronal communication through neuronal coherence. Trends. Cogn. Sci. 9 (10), 474–480. https://doi.org/10.1016/j.tics.2005.08.011.

Fries, P., Nikolić, D., Singer, W., 2007. The gamma cycle. Trends. Neurosci. 30 (7), 309–316. https://doi.org/10.1016/j.tins.2007.05.005.

García-Rosales, F., Martin, L.M., Beetz, M.J., Cabral-Calderin, Y., Kössl, M., & Hechavarria, J.C. (.2018). Low-Frequency Spike-Field Coherence Is a Fingerprint of Periodicity Coding in the Auditory Cortex. *iScience*, 9, 47–62. https://doi.org/10.1016/j.isci.2018.10.009.

García-Rosales, F., López-Jury, L., González-Palomares, E., Cabral-Calderín, Y., Kössl, M., Hechavarria, J.C., 2020. Phase-amplitude coupling profiles differ in frontal and auditory cortices of bats. European Journal of Neuroscience. https://onlinelibrary.wiley.com/doi/pdfdirect/10.1111/ejn.14986.

Giraud, A.-L., Poeppel, D., 2012. Cortical oscillations and speech processing: emerging computational principles and operations. Nat. Neurosci. 15 (4), 511–517. https://doi.org/10.1038/nn.3063.

Groppe, D.M., Urbach, T.P., Kutas, M., 2011a. Mass univariate analysis of event-related brain potentials/fields I: a critical tutorial review. Psychophysiology. 48 (12), 1711–1725. https://doi.org/10.1111/j.1469-8986.2011.01273.x.

Groppe, D.M., Urbach, T.P., Kutas, M., 2011b. Mass univariate analysis of event-related brain potentials/fields II: simulation studies. Psychophysiology. 48 (12), 1726–1737. https://doi.org/10.1111/j.1469-8986.2011.01272.x.

Handa, T., Takekawa, T., Harukuni, R., Isomura, Y., Fukai, T., 2017. Medial Frontal Circuit Dynamics Represents Probabilistic Choices for Unfamiliar Sensory Experience. Cereb. Cortex. 1–14. https://doi.org/10.1093/cercor/bhx031.

Harris, K.D., Bartho, P., Chadderton, P., Curto, C., de la Rocha, J., Hollender, L., Itskov, V., Luczak, A., Marguet, S.L., Renart, A., Sakata, S., 2011. How do neurons work together? Lessons from auditory cortex. Hear. Res. 271 (1–2), 37–53. https://doi.org/10.1016/j.heares.2010.06.006.

Heid, S., Hartmann, R., Klinke, R., 1998. A model for prelingual deafness, the congenitally deaf white cat–population statistics and degenerative changes. Hear. Res. 115 (1–2), 101–112. PubMed.

Herrmann, C.S., Rach, S., Vosskuhl, J., Strüber, D., 2014. Time-frequency analysis of event-related potentials: a brief tutorial. Brain Topogr. 27 (4), 438–450. https://doi.org/10.1007/s10548-013-0327-5.

Hyafil, A., Giraud, A.-L., Fontolan, L., Gutkin, B., 2015. Neural Cross-Frequency Coupling: connecting Architectures, Mechanisms, and Functions. Trends. Neurosci. 38 (11), 725–740. https://doi.org/10.1016/j.tins.2015.09.001.

Kaminska, A., Delattre, V., Laschet, J., Dubois, J., Labidurie, M., Duval, A., Manresa, A., Magny, J.-F., Hovhannisyan, S., Mokhtari, M., Ouss, L., Boissel, A., Hertz-Pannier, L., Sintsov, M., Minlebaev, M., Khazipov, R., Chiron, C., 2017. Cortical Auditory-Evoked Responses in Preterm Neonates: revisited by Spectral and Temporal Analyses. Cereb. Cortex. 1–16. https://doi.org/10.1093/cercor/bhx206.

Köster, M., Martens, U., Gruber, T., 2019. Memory entrainment by visually evoked theta-gamma coupling. Neuroimage 188, 181–187. https://www.sciencedirect.com/science/article/pii/S1053811918321463?casa_token=pX9rJuNYbZoAAAAA:Go6E5ueQ3mHRcTE03hfQWtAFB5c9sh8LKTlQGj5PRywD5XLAt7oOHkYzfe6nLuLnPFktp7Uurdo.

Kral, A., Dorman, M.F., Wilson, B.S., 2019. Neuronal Development of Hearing and Language: cochlear Implants and Critical Periods. Annu Rev. Neurosci. 42, 47–65. https://doi.org/10.1146/annurev-neuro-080317-061513.
Kral, A., Hartmann, R., Tillein, J., Heid, S., Klinke, R., 2000. Congenital auditory deprivation reduces synaptic activity within the auditory cortex in a layer-specific manner. Cereb. Cortex. 10 (7), 714–726.
Kral, A., Hartmann, R., Tillein, J., Heid, S., Klinke, R., 2002. Hearing after congenital deafness: central auditory plasticity and sensory deprivation. Cereb. Cortex. 12 (8), 797–807.
Kral, A., Heid, S., Hubka, P., Tillein, J., 2013a. Unilateral hearing during development: hemispheric specificity in plastic reorganizations. Front. Syst. Neurosci. 7, 93. https://doi.org/10.3389/fnsys.2013.00093.
Kral, A., Tillein, J., Hartmann, R., Klinke, R., 1999. Monitoring of anaesthesia in neurophysiological experiments. Neuroreport 10 (4), 781–787.
Kral, A., Tillein, J., Heid, S., Hartmann, R., Klinke, R., 2005. Postnatal Cortical Development in Congenital Auditory Deprivation. Cereb. Cortex. 15, 552–562.
Kral, A., Tillein, J., Heid, S., Klinke, R., Hartmann, R., 2006. Cochlear implants: cortical plasticity in congenital deprivation. Prog. Brain Res. 157, 283–313.
Kral, A., 2013. Auditory critical periods: a review from system's perspective. Neuroscience 247, 117–133. https://doi.org/10.1016/j.neuroscience.2013.05.021.
Kral, A., Hubka, P., Heid, S., Tillein, J., 2013b. Single-sided deafness leads to unilateral aural preference within an early sensitive period. Brain 136 (Pt 1), 180–193. https://doi.org/10.1093/brain/aws305.
Kral, A., Kronenberger, W.G., Pisoni, D.B., O'Donoghue, G.M, 2016. Neurocognitive factors in sensory restoration of early deafness: a connectome model. Lancet Neurol. 15 (6), 610–621. https://doi.org/10.1016/S1474-4422(16)00034-X.
Kral, A., Sharma, A., 2023. Crossmodal plasticity in hearing loss. Trends Neurosci. 46 (5), 377–393. https://www.cell.com/trends/neurosciences/fulltext/S0166-2236(23)00045-0.
Kral, A., Tillein, J., Hubka, P., Schiemann, D., Heid, S., Hartmann, R., Engel, A.K., 2009. Spatiotemporal patterns of cortical activity with bilateral cochlear implants in congenital deafness. J. Neurosci. 29 (3), 811–827. https://doi.org/10.1523/JNEUROSCI.2424-08.2009.
Lakatos, P., Shah, A.S., Knuth, K.H., Ulbert, I., Karmos, G., Schroeder, C.E., 2005. An oscillatory hierarchy controlling neuronal excitability and stimulus processing in the auditory cortex. J. Neurophysiol. 94 (3), 1904–1911. https://doi.org/10.1152/jn.00263.2005.
Leicht, G., Björklund, J., Vauth, S., Mußmann, M., Haaf, M., Steinmann, S., Rauh, J., Mulert, C., 2021. Gamma-band synchronisation in a frontotemporal auditory information processing network. Neuroimage 239, 118307. https://doi.org/10.1016/j.neuroimage.2021.118307.
Lisman, J.E., Jensen, O., 2013. The θ-γ neural code. Neuron 77 (6), 1002–1016. https://doi.org/10.1016/j.neuron.2013.03.007.
MacDonald, K.D., Barth, D.S., 1995. High frequency (gamma-band) oscillating potentials in rat somatosensory and auditory cortex. Brain Res. 694 (1–2), 1–12. PubMed.
Mallat, S.G., Zhang, Z., 1993. Matching pursuits with time-frequency dictionaries. IEEE Transactions on signal processing 41 (12), 3397–3415. https://ieeexplore.ieee.org/abstract/document/258082.
Manini, B., Vinogradova, V., Woll, B., Cameron, D., Eimer, M., Cardin, V., 2022. Sensory experience modulates the reorganization of auditory regions for executive processing. Brain awac205. https://doi.org/10.1093/brain/awac205.
Mercier, M.R., Molholm, S., Fiebelkorn, I.C., Butler, J.S., Schwartz, T.H., Foxe, J.J., 2015. Neuro-oscillatory phase alignment drives speeded multisensory response times: an electro-corticographic investigation. J. Neurosci. 35 (22), 8546–8557. https://doi.org/10.1523/JNEUROSCI.4527-14.2015.
Michael, E., Covarrubias, L.S., Leong…, V., 2023. Learning at your brain's rhythm: individualized entrainment boosts learning for perceptual decisions. Cerebral Cortex. https://academic.oup.com/cercor/article/33/9/5382/6814397?login=false.
Morillon, B., Liégeois-Chauvel, C., Arnal, L.H., Bénar, C.-G., Giraud, A.-L., 2012. Asymmetric function of theta and gamma activity in syllable processing: an intra-cortical study. Front. Psychol. 3, 248. https://doi.org/10.3389/fpsyg.2012.00248.
Oostenveld, R., Fries, P., Maris, E., Schoffelen, J.-M., 2011. FieldTrip: open source software for advanced analysis of MEG, EEG, and invasive electrophysiological data. Comput. Intell. Neurosci. 2011, 156869 https://doi.org/10.1155/2011/156869.
Ponton, C.W., Eggermont, J.J., 2001. Of Kittens and Kids: altered Cortical Maturation following Profound Deafness and Cochlear Implant Use. Audiol. Neurootol. 6 (6), 363–380.
Ray, S., Maunsell, J.H.R., 2011. Different origins of gamma rhythm and high-gamma activity in macaque visual cortex. PLoS. Biol. 9 (4), e1000610. https://journals.plos.org/plosbiology/article?id=10.1371/journal.pbio.1000610.
Sato, M., Baumhoff, P., Kral, A., 2016. Cochlear Implant Stimulation of a Hearing Ear Generates Separate Electrophonic and Electroneural Responses. J. Neurosci. 36 (1), 54–64. https://doi.org/10.1523/JNEUROSCI.2968-15.2016.
Sato, M., Baumhoff, P., Tillein, J., Kral, A., 2017. Physiological Mechanisms in Combined Electric-Acoustic Stimulation. Otol. Neurotol. 38 (8), e215–e223. https://doi.org/10.1097/MAO.0000000000001428.
Schiecke, K., Wacker, M., Benninger, F., Feucht, M., Leistritz, L., Witte, H., 2015. Matching pursuit-based time-variant bispectral analysis and its application to biomedical signals. IEEE Transactions on Biomedical Engineering 62 (8), 1937–1948. https://ieeexplore.ieee.org/abstract/document/7050302.
Schroeder, C.E., Lakatos, P., 2009. Low-frequency neuronal oscillations as instruments of sensory selection. Trends. Neurosci. 32 (1), 9–18. https://doi.org/10.1016/j.tins.2008.09.012.
Sedley, W., Gander, P.E., Kumar, S., Kovach, C.K., Oya, H., Kawasaki, H., Howard, M.A., Griffiths, T.D., 2016. Neural signatures of perceptual inference. Elife 5. https://doi.org/10.7554/eLife.11476.
Senkowski, D., Pomper, U., Fitzner, I., Engel, A.K., Kral, A., 2014. Beta-band activity in auditory pathways reflects speech localization and recognition in bilateral cochlear implant users. Hum. Brain Mapp. 35 (7), 3107–3121. https://doi.org/10.1002/hbm.22388.
Sharma, A., Dorman, M.F., Kral, A., 2005. The influence of a sensitive period on central auditory development in children with unilateral and bilateral cochlear implants. Hear. Res. 203 (1–2), 134–143.
Siegel, M., Donner, T.H., Engel, A.K., 2012. Spectral fingerprints of large-scale neuronal interactions. Nat. Rev. Neurosci. 13 (2), 121–134. https://doi.org/10.1038/nrn3137.
Singer, W., 2011. Dynamic Formation of Functional Networks by Synchronization. Neuron 69 (2), 191–193. https://doi.org/10.1016/j.neuron.2011.01.008.
Suárez, L.E., Markello, R.D., Betzel, R.F., Misic, B., 2020. Linking Structure and Function in Macroscale Brain Networks. Trends. Cogn. Sci. 24 (4), 302–315. https://doi.org/10.1016/j.tics.2020.01.008.
Sukov, W., Barth, D.S., 2001. Cellular mechanisms of thalamically evoked gamma oscillations in auditory cortex. J. Neurophysiol. 85 (3), 1235–1245.
Tallon-Baudry, C., Bertrand, O., Delpuech, C., Permier, J., 1997. Oscillatory gamma-band (30-70 Hz) activity induced by a visual search task in humans. J. Neurosci. 17 (2), 722–734.
Tallon-Baudry, C., Bertrand, O., Delpuech, C., Pernier, J., 1996. Stimulus specificity of phase-locked and non-phase-locked 40 Hz visual responses in human. J. Neurosci. 16 (13), 4240–4249.
Tillein, J., Hubka, P., Syed, E., Hartmann, R., Engel, A.K., Kral, A., 2010. Cortical representation of interaural time difference in congenital deafness. Cereb. Cortex. 20 (2), 492–506. https://doi.org/10.1093/cercor/bhp222.
Tort, A.B.L., Komorowski, R., Eichenbaum, H., Kopell, N., 2010. Measuring phase-amplitude coupling between neuronal oscillations of different frequencies. J. Neurophysiol. 104 (2), 1195–1210. https://journals.physiology.org/doi/full/10.1152/jn.00106.2010.
Tsunada, J., Baker, A.E., Christison-Lagay, K.L., Davis, S.J., Cohen, Y.E., 2011. Modulation of cross-frequency coupling by novel and repeated stimuli in the primate ventrolateral prefrontal cortex. Front. Psychol. 2, 217. https://doi.org/10.3389/fpsyg.2011.00217.
Uhlhaas, P.J., Roux, F., Singer, W., Haenschel, C., Sireteanu, R., Rodriguez, E., 2009. The development of neural synchrony reflects late maturation and restructuring of functional networks in humans. Proc. Natl. Acad. Sci. u S. a 106 (24), 9866–9871. https://doi.org/10.1073/pnas.0900390106.
van de Nieuwenhuijzen, M.E., Axmacher, N., Fell, J., Oehrn, C.R., Jensen, O., van Gerven, M.A.J., 2016. Decoding of task-relevant and task-irrelevant intracranial EEG representations. Neuroimage 137, 132–139. https://doi.org/10.1016/j.neuroimage.2016.05.008.
van Driel, J., Cox, R., Cohen, M.X., 2015. Phase-clustering bias in phase-amplitude cross-frequency coupling and its removal. J. Neurosci. Methods 254, 60–72. https://doi.org/10.1016/j.jneumeth.2015.07.014.
von Nicolai, C., Engler, G., Sharott, A., Engel, A.K., Moll, C.K., Siegel, M., 2014. Corticostriatal coordination through coherent phase-amplitude coupling. J. Neurosci. 34 (17), 5938–5948. https://doi.org/10.1523/JNEUROSCI.5007-13.2014.
Widmann, A., Gruber, T., Kujala, T., Tervaniemi, M., Schröger, E., 2007. Binding symbols and sounds: evidence from event-related oscillatory gamma-band activity. Cereb. Cortex. 17 (11), 2696–2702. https://doi.org/10.1093/cercor/bhl178.
Wöstmann, M., Lim, S.-J., Obleser, J., 2017. The Human Neural Alpha Response to Speech is a Proxy of Attentional Control. Cereb. Cortex. 27 (6), 3307–3317. https://doi.org/10.1093/cercor/bhx074.
Yusuf, P.A., Hubka, P., Tillein, J., Kral, A., 2017. Induced Cortical Responses Require Developmental Sensory Experience. Brain 140 (12), 3153–3165.
Yusuf, P.A., Hubka, P., Tillein, J., Vinck, M., Kral, A., 2021. Deafness weakens interareal couplings in the auditory cortex. Front. Neurosci. 14, 1476. https://www.frontiersin.org/articles/10.3389/fnins.2020.625721/full.
Yusuf, P.A., Lamuri, A., Hubka, P., Tillein, J., Vinck, M., Kral, A., 2022. Deficient Recurrent Cortical Processing in Congenital Deafness. Front. Syst. Neurosci. 16, 806142. https://www.ncbi.nlm.nih.gov/pmc/articles/PMC8913535.